www.ijecs.in
International Journal Of Engineering And Computer Science ISSN:2319-7242
Volume 3 Issue 11 November, 2014 Page No. 9313-9322

Automated 3d-Image Extraction in Brain MRI Using Geometric Transformable Prototype

D Chamundeshwari [1], J Thirupathi [2], J Srinivas [3]

[1] **Mrs. D Chamundeshwari**, Assoc. Professor in Department of Electronics and Communication Engineering, Elenki Institute of Engineering and Technology, JNTU Hyderabad, INDIA,, E-mail: dasaris.chamu@gmail.com

[2]**Mr. J Thirupathi,** Assoc. Professor in Department of Computer Science and Engineering, College of Engineering and Technology, Samara University, Samara, ETHIOPIA, E-mail: thirupathij.cse@gmail.com

[3]**Mr. J Srinivas** M.Tech (Embedded Systems)II Year, RRS Engineering College. JNTU Hyderabad, INDIA.

Abstract: *This paper describes a new method called adaptive hybrid Transformable geometric segmentation that uses knowledge of tissue intensity properties and intensity in-homogeneities to correct and segment MR images. Use of the expectation-maximization (EM) algorithm leads to a method that allows for more accurate segregation of tissue types as well as better visualization of magnetic resonance imaging (MRI) data, we have described an unsupervised fuzzy segmentation method, based on new objective function, which seems well adapted and efficient for functional MRI data segregation. The proposed segmentation method is more robust than the FCM algorithm and BCFCM. The proposed segmentation uses an automatic algorithm for robust WM, GM, and cerebrospinal fluid (CSF) segmentation to facilitate accurate measurement of brain tissues. Both qualitative and quantitative results on synthetic and real brain MRI scans indicate superior and consistent performance. One popular family of brain tissue segregation methods is based on normalizing the brain scans by storing (or aligning) them to a pre defined realistic view of brain tissues.*

Keywords: magnetic resonance imaging (MRI), Brain Mask, Brain Extraction.

1. Introduction

The term digital image refers to processing of a two dimensional picture by a digital computer. In a broader context, it implies digital processing of any two dimensional data. A digital image is an array of real or complex numbers represented by a finite number of bits. An image given in the form of a transparency, slide, photograph or an X-ray is first digitized and stored as a matrix of binary digits in computer memory.

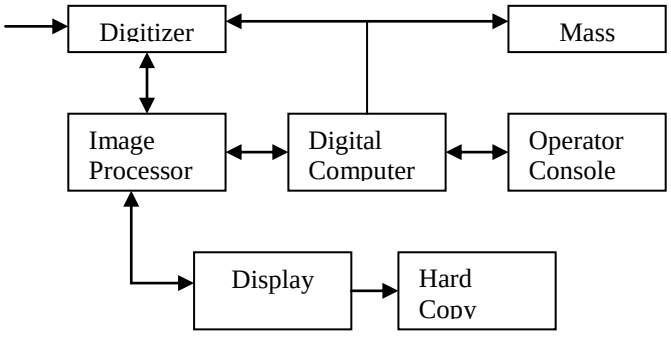

Block Diagram of a Typical Image Processing

Digitizer A digitizer converts an image into a numerical representation suitable for input into a digital computer. Some common digitizers are

1. Microdensitometer
2. Flying spot scanner
3. Image dissector
4. Videocon camera
5. Photosensitive solid- state arrays.

Mass Storage The secondary storage devices normally used are floppy disks, CD ROMs etc.

Image Processor An image processor does the functions of image acquisition, storage, preprocessing, segregation, representation, recognition and interpretation and finally displays or records the resulting image. The following block diagram gives the fundamental sequence involved in an image processing system

Digital Computer Mathematical processing of the digitized image such as convolution, averaging, addition, subtraction, etc. are done by the computer.

Hard Copy Device The hard copy device is used to produce a permanent copy of the image and for the storage of the software involved.

Operator Console The operator console consists of equipment and arrangements for verification of intermediate results and for alterations in the software as and when require. The operator is also capable of checking for any resulting errors and for the entry of requisite data.

Magnetic resonance (MR) has become the main modality for brain imaging that facilitates safe, noninvasive assessment and monitoring of patients with neurodegenerative diseases such as Parkinson's disease, Alzheimer's disease (AD), epilepsy, schizophrenia, and multiple sclerosis (MS). The ability to diagnose and characterize these diseases in vivo using MR image data promises exciting developments both toward understanding the underlying pathologies, as well as conducting clinical trials of drug treatments. One important biomarker that is often used to assess patients with neuro-de generative disease is brain tissue volume. The typical rate of global brain atrophy in MS patients has been shown to be 0.6%– 0.8% annually, which is two to three times the normal

atrophy rate. Evidence has shown that white matter (WM) and gray matter (GM) atrophy at different rates, and each correlates differently to disability thus, accurate measurement of the WMand GMbrain tissues can provide valuable quantitative indicators of disease progression and, potentially, treatment out- comes. Thus, the main aim of this paper is to introduce an automatic algorithm for robust WM, GM, and cerebrospinal fluid (CSF) segregation to provide accurate measurement of brain tissues.

A second family of brain tissue segregation methods assigns a label for each tissue based on image statistics either by clustering or by modeling the brain tissue intensity distributions as a finite mixture of distributions such as EM , maximum a posteriori (MAP), simulated annealing , and Gaussian mixture modeling (GMM). Other approaches incorporate additional regional information, which is lacking from these statistical methods, into their segregation frame-work. Such methods extend clustering or EM by integrating with fuzzy connectedness, topological constraints,

Gibbs random field (GRF), and hidden Markov random field (HMRF) in the segmentation task. A common difficulty with many of these methods, particularly the random field approaches, is the requirement for proper parameter settings in a supervised setting.

A third family of brain tissue segregation methods is based on utilizing geometric information such as transformable prototypes or active contours that delineates region boundaries using a minimization of an energy functional . Transformable prototypes employing level sets provide an effective implicit representation rather than explicit parameterization of the evolving contour. However, a common problem of directly applying the active contour approach in segmenting brain MR images is leakage through weak or noisy edges that are ubiquitous, especially for edge-based Transformable prototypes,

2. Literature Survey

An MRI study of patients with Parkinson's disease with mild cognitive impairment and dementia using voxel based morphometry.

We studied regional gray matter density in the hippocampus in Parkinson's disease (PD) patients. We obtained magnetic resonance scans in 44 PD patients (PD patients with dementia (PDD) = 9, non-demented PD patients with visual hallucinations (PD + VH) = 16, and PD patients without dementia and without visual hallucinations (PD - VH) = 19) and 56 controls matched for age and years of education. A region of interest (ROI) of the hippocampus following voxel-based-morphometry (VBM) procedures was used to perform group comparisons, single-case individual analysis and correlations with learning scores. Group comparisons showed that PDD patients and PD+VH patients had significant hippocampus gray matter loss compared to controls. In PDD patients, hippocampus gray matter loss involved the entire hippocampus and in PD+VH this reduction was mainly confined to the hippocampus head. 78 % of PDD patients, 31 % of PD+VH patients and 26 % of PD-VH patients had hippocampus head gray matter loss when compared to controls. These results suggest that in PD the neurodegenerative process in the hippocampus starts in the head of this structure and later spreads to the tail and that, in addition, memory impairment assessed by Rey's Auditory Verbal Learning Test (RAVLT) correlates with hippocampus head gray matter loss.

2.1 Neuro Imaging In Multiple Sclerosis

MRI is the dominant neuro imaging modality for multiple sclerosis (MS). Revised diagnostic criteria formally incorporate abnormalities on MRI for diagnosis. MRI is well-suited for evaluating dynamic changes in MS patients. This paper reviews how conventional and advanced MRIs provide important biomarkers of MS pathology and considers the role of MRI outcomes in clinical trials and in clinical practice.

2.2 Current Methods In Automatic Tissue Segregation Of 3d Magnetic Resonance Brain Images

To improve the efficiency of brain image analysis, we propose a full-automatic method for extracting brain tissue from three-dimensional magnetic resonance imaging of T1-weighted data on the human head. The extraction processing is realized by combining signal intensity thresholding by means of the discriminate analysis method and an erosion-dilation treatment of the image. The accuracy of BREED is evaluated using both simulated and subject data. BREED can extract brain tissues with high approximate 97% for either simulated or subject data.

2.3 Adaptive Fuzzy Segregation of MRI

A new approach for robust segregation of magnetic resonance images is described. The approach is derived from a generalization of the objective function used in Pham and Prince's Adaptive Fuzzy C-means algorithm (AFCM). Within the objective function, an additional constraint is placed on the membership function that forces them to be spatially smooth. The efficacy of the algorithm is demonstrated on simulated magnetic resonance images.

2.4 Adaptive Segregation of MRI Data

Intensity-based classification of MR images has proven problematic, even when advanced techniques are used. Intra scan and inter scan intensity inhomogeneities are a common source of difficulty. While reported methods have had some success in correcting intra scan inhomogeneities, such methods require supervision for the individual scan. This paper describes a new method called adaptive segregation that uses knowledge of tissue intensity properties and intensity inhomogeneities to correct and segment MR images. Use of the expectation-maximization (EM) algorithm leads to a method that allows for more accurate segregation of tissue types as well as better visualization of magnetic resonance imaging (MRI) data, that has proven to be effective in a study that includes more than 1000 brain scans. Implementation and results are described for segmenting the brain in the following types of images: axial (dual-echo spin-echo), coronal [three dimensional Fourier transform (3-DFT) gradient-echo T1-weighted] all using a conventional head coil, and a sagittal section acquired using a surface coil. The accuracy of adaptive segregation was found to be comparable with manual segregation, and closer to manual segregation than supervised multivariate classification while segmenting gray and white matter.

3. Design Methodology

In this paper we proposed a 3-D brain MR segregation method based on Transformable prototypes and demonstrated accurate and stable brain tissue segregation on single as well as multiple MR sequence scans.

3.1 Module Separation

Module 1: Edge based Transformable prototype.
Module 2: hybrid geometric statistical feature.
Module 3: Segregation of brain MRI.
Module 4: Extension to multiple MRI.

Module 1: Edge Based Transformable Prototype

In first module, we utilize the geodesic active contour prototype Rather than the region-based formulation due to its Computation soundness and extendibility. The value of this feature function determines the propagation of the surface by searching for the minimal Riemannian distance. An ideal edge would ultimately have a feature value of zero at all the pixel points along this boundary. This process is subjective and ideal parameters are often difficult to derive for a fully automated segregation framework.

Module 2: Proposed Hybrid Geometric Statistical Feature

In this module to transform the feature function g in the traditional geodesic active contour formulation into a hybrid feature function by incorporating geometric image features with voxel statistics to help automate and regularize the evolving contours. This parameter estimation problem for GMM solved by employ EM algorithm to image intensity histogram.

Module 3: Segregation of Brain MRI

To segment the brain tissues, we first estimate the GMM parameters such that each mixture distribution represents one single class. Based on these estimated distributions, the normalized posterior probability of each voxel is calculated. We derive the hybrid geometric–statistical feature as described above by combining both the voxel statistics and the image gradient information.

Module 4: Extension to Multiple MRI

We extend our method so that information from multiple MR sequences with different contrast properties can be incorporated when the data is available. Assuming registered images, we first replace the geometric feature component in the proposed hybrid active contour feature with the multidimensional vector gradient norm derived from all available data sequences. The resulting probability replaces the posterior probability derived from single contrast input in the segregation procedure.

4. Design Analysis

The accurate and effective algorithm for segmenting image is very useful in many fields, especially in medical image. In this paper we introduced a novel method that focus on segmenting the brain MR Image that is important for neural diseases. Because of many noises embedded in the acquiring procedure, such as eddy currents, susceptibility artifacts, rigid body motion, and intensity in homogeneity, segmenting the brain MR image is a difficult work. In this algorithm, we overcame the inhomogeneous shortage, by modifying the objective function with compensating its immediate neighborhood effect using Gaussian smooth method for decreasing the influence of the in homogeneity and increasing the segmenting accuracy. With simulate image and the clinical MRI data, the experiments shown that our proposed algorithm is effective.

4.1 Methods

4.1.1 Prototype of Fuzzy C-Mean Method (FCM)

The standard FCM is an iterative, unsupervised clustering algorithm, initially developed by FCM algorithm, introduced by Bezdek. The following prototype of FCM is described by Ahmed.

The Observed MRI signal is modeled as a product of the true signal generated by the underlying anatomy, and a spatially varying factor called the gain field

$$Y_k = X_k G_k \quad \forall k \in \{1, 2, \cdots, N\}$$

Groups the values X_k, Y_k and G_k are the true intensity, observed intensity and the gain field at the *k*th voxel, respectively. N is the total number of pixels in the MRI volume.The application of a logarithmic transformation to the intensities allows the artifact to be modeled as an additive bias field

$$y_k = x_k + \beta_k \qquad \forall k \in \{1, 2, \cdots, N\}$$

Where x_k and y_k are the true and observed log-transformed intensities at the *k*th voxel, respectively, and β_k is the bias field at the *k*th voxel. If the gain field is known, then it is relatively easy to estimate the tissue class by applying a conventional intensity-based segregation to the corrected data. The following discussion is based the model of (2) and estimation of the gain field β_k .

4.1.2 Modified Fcm Algorithm (M-Fcm)

In the followings, we will introduce some modifications to this algorithm. The evaluation of the method for localized measurements, such as the impact on tumor boundary or volume determinations also needs further work.

$$J_m = \sum_{i=1}^{c} \sum_{k=1}^{N} u_{ik}^{p} \| y_k - \beta_k - v_i \|^2 + \sum_{i=1}^{c} \sum_{k=1}^{N} u_{ik}^{p} \Big(\sum_{y_r \in N_k} w(y_k, y_r) \| y_r - \beta_r - v_i \|^2 \Big)$$

Where $w(y_k, y_r)$ is a weighting function, satisfied the following conditions

$$\sum_{y_r \in N_k} w(y_k, y_r) = \alpha, \qquad 0 \le \alpha < 1,$$

$\forall k \in \{1, 2, \cdots, N\}$ especially, when $w(y_k, y_r) = \dfrac{\alpha}{N_R}$,

the J_m is BCFCM objective function (3) proposed by Ahmed. The objective function can be calculated as the BCFCM algorithm. Taking the first derivatives of J_m with respect to u_{ik} , v_i , β_k , and setting them to zero results in three necessary but not sufficient conditions for J_m to be at a local maximum. In the following sections, we derive these estimating results and propose the algorithm.

The M-FCM algorithm for correcting the bias field and segmenting the image into different clusters can be summarized in the following steps.

Step 1: Select the Weighting function, in general,

$$w(y_k - y_r) = \alpha e^{-\frac{\|y_k - y_r\|^2}{\sigma^2}} \quad \text{Where } 0 \le \alpha < 1, \sigma \ge 1;$$

Step 2: Select initial class prototypes $\{v_i\}_{i=1}^{c}$, for example

$$\left\{ v_i = \log(255 * (2i-1)/2c) \right\}_{i=1}^{c} \quad \text{Set } \{\beta_k\}_{k=1}^{N} \text{ to equal and}$$

very small values (e.g., 0.01).

Step 3: Update the partition matrix using.

Step 4: The prototypes of the clusters are obtained in the form of weighted averages of the patterns using.

Step 5: Estimate the bias term using. Repeat Steps 3 and 5 till termination.

In this section, we describe the application of the M-FCM segregation on synthetic images corrupted with multiplicative gain and real T1 brain MR images. For compared with the BCFCM algorithm, we created the simulating image used by Ahmed. Simulating image is a T1-weighted phantom with in-plane high resolution, Gaussian noise with 6.0, and three-dimensional linear shading 7% in each direction. We also employed the fast algorithm for improving calculation effect, because its consumed time is 1/4 of the normal algorithm.

We applied our proposed segregation to both simulated and real clinical MRI scans, and demonstrated in the following sections:

1) The accuracy of the proposed segregation method on simulated T1w brain MRIs.

2) The segregation improvement on multiple MRI sequences.

3) The accuracy of the proposed method on real clinical MRI scans of normal adults.

4) The qualitative performance of the proposed methods on clinical MRI scans of MS and AD patients.

We first validated our proposed method on 18 simulated T1w Brain Web MRI images (with 0%/1%/3%/5%/7%/9% noise, 0%/20%/40% in homogeneity, 181 × 217 × 181 dimension, 1 × 1 × 1 mm3 spacing). We also performed multi-sequence segregation based on six T1w/T2w/PD w MRI triplets (with 0%/1%/3%/5%/7%/9% noise, 0% in homogeneity). Second, 18 real high-resolution clinical T1w MRI scans from the Internet Brain Segmentation Repository (IBSR) (coronals acquired, 256 × 128 × 256 dimension, 0.837 × 0.837 mm2 to 1 × 1 mm2 in-plane spacing, 1.5 mm slice thickness) were also segmented. For both datasets, the "ground truth" is known for comparisons. For the Brain Web dataset, the ground truth is the phantom atlas used to generate the simulated scans, whereas for the IBSR dataset, the truth is the provided expert-guided manual segregation label for each of the clinical scans.

The method was tested on the data from eight patients with total manual infected volumes ranging from 200 to 28000 mm3 Each data set had dual echo PD and T2 images. The manual segregation of the data was done independently by a trained technologist. The automatic segregation results were analyzed by comparisons with the manual segregation of the same scans, using similarity index and total infected volume correlation figures. Results show a total volume correlation of 0.972.

Lastly, from the MSMRI Research Group (MS/MRI), real clinical 1.5 T spoiled gradient (SPGR) MRI scans (axially acquired, 256 × 256×120–160 dimension, 0.937×0.937×1.50mm3 spacing) were taken at multiple sites. Real clinical 1.5 T magnetization prepared rapid gradient echo (MP-RAGE) MRI scans (Sagittally acquired, 256 × 256 × 166 dimension, 0.937 × 0.937 × 1.20mm3 spacing) were also obtained from the AND euro imaging Initiative (ADNI) of the LONI image data archive (IDA) initiated by the National Institute on Aging (NIA), the National Institute of Biomedical Imaging and Bioengineering (NIBIB), the Food and Drug Administration (FDA), private pharmaceutical companies, and nonprofit organizations. These clinical scans were segmented and qualitatively evaluated. The average surface distance between the ground truth and the computed segregation was computed for each test scan by approximate nearest neighbor searching. In addition, the Dice similarity index was also chosen for the quantitative evaluation of the 3-D brain segregation results to facilitate direct comparisons to other published results Dice similarity index 2T+ 2T+ + F+ + F− × 100%. We denote the true positives, true negatives, false positives, and false negatives as T+, T−, F+, and F−, respectively, between the known ground truth and the segregation results. We compared our segregation results with those of the M3DLS method.

4.1.3 Segregation Validation Using Simulated Brain MRI

We first validated a three-class (WM, GM, and CSF) segregation using the proposed method on the simulated T1w brain MRI data. Segregation was performed using the traditional geometric feature only, the statistical in homogeneity levels. For the edge-only level set evolution the parameter set {ψ = 2.0, c = 1.0, ε = 4.5} was used to enforce a stronger smoothness constrain; otherwise, contours leaking through weak edges were often observed. For the statistical feature term only, the parameter set {ψ = 0.0, c = 1.0 ε = 0.0} was used, same as the hybrid approach. Segregation of structures such as CSF by using the proposed approach also achieved considerable (>70%) similarity of 77.75% (σ = 6.15%, average distance = 2.24 mm). The CSF results were not as stable as WM and GM mainly due to the much smaller structural volume, leading to increased sensitivity to estimation errors in the active contour initialization and feature derivation. Nonetheless, the overall segregation results were on par if not better than other previously published results.

To statistically evaluate the differences of segregation results between the proposed hybrid approach, and the contours based on geometric-only and statistical-only features, we calculated the p-values ($p < 0.05$ indicates a statistically significant difference in the group means). Compare to results from using only the traditional geometric feature, the proposed hybrid approach achieved significantly higher similarity indexes and reduced surface distance across all scans. On average, the proposed method achieved increased similarity indexes of 5.36% ($p = 0.0002$) in WM, 7.23% ($p < 0.0001$) in GM, and 9.30% ($p < 0.0001$) in CSF segregation results with reduced surface distance of 3.99 mm ($p < 0.0001$) in WM, 0.27 mm ($p < 0.0001$) in GM, and 4.86 mm ($p < 0.0001$) in CSF. Compare to results from using only the statistical feature, the proposed

hybrid approach only achieved slightly better similarity indexes. However, we observed that, on average, the proposed method was able to significantly reduce the average surface distance by 4.44mm ($p<0.0001$) in WM and 3.79mm ($p<0.0001$) in CSF.

These results showed that using the geometric term alone was highly sensitive to image artifacts and require contour regularization. Processing a single Brain Web volume takes approximately 55 min (dual 3.20 GHz Xeon PC with 3.25 GB memory) to 75 min (3.60 GHz Pentium4 PC with 2GBmemory), comparable to the processing time required by other conventional techniques.

4.1.4 Segregation Improvement Using Multiple MRI Sequences

We next performed a three-class (WM, GM, and CSF) segregation using the proposed method on the simulated T1w/T2w/PD w brain MRI data. Segregation was performed on six datasets with varying noise levels and 0% intensity In homogeneity. Qualitative results in Fig. illustrated very good resemblance between the provided phantom label and the segregation results. When compared to the experiment on single simulated T1w brain images, segregation using multiple MR sequence data provided an average improvement in similarity indexes of 1.29% ($p = 0.0479$), 0.44% ($p = 0.4627$), and 3.55% ($p = 0.1403$) for WM, GM, and CSF, respectively.

Additional MR sequences such as T2w and PD win this case, helpful to improve the overall robustness by achieving a much better balance between the WM, GM, and CSF estimation as observed by the T+ and T− performance.

4.1.5 Segregation Comparisons Using Clinical MRI Scans of Normal Adults

We applied the proposed method to segment 18 clinical IBSR brain images. The images were segmented using a three-class (WM, GM, and CSF) segregation. The tissue labels were then post processed due to a known limitation of the provided manual segregation labels. It has been reported previously that the expert guided manual segregation label contains much of the cortical CSF being mislabeled as GM. We have confirmed this with our own observations. As observed, we note that the original segregation results matched closely with what can be visually observed from the raw images. However, this observation did not correspond well to the provided expert guided manual segregation label due to the existing limitation.

4.1.6 Segregation Performance Using Clinical MRI Scans Of Ms and Ad Patients

Lastly, we applied the proposed method to segment clinical MRI brain scans of MS and AD patients. The images were segmented using a three-class (normal appearing WM, GM grouped with diseased WM, and CSF) segregation. The qualitative results demonstrating that the proposed approach appears stable on clinical scans.

In our T1w test scans, the intensity difference between GM and diseased WM is subtle, and separating these two class types is likely not possible without additional MRI sequences that are more sensitive to WM pathology, such as PD w or T2w, or relying on prior probability maps such as those derived from a training set. We have left these experiments for future work. In its current form, the proposed method can potentially be used for the assessment of disease severity by providing stable and consistent segregations of CSF and normal appearing WM.

Where the TR is the percent of divided segregation umbers of WM pixels by number of original all the WM pixels. Table display TR that can explain the performance of those algorithms with different noise level.

TR	*SNR*			
	None	5db	10db	13db
FCM	89.24	85.46	79.30	75.46
BCFCM	96.76	91.10	84.32	82.10
M-FCM	98.20	96.23	91.57	90.46

Segregation accuracy-TR of different methods with different noise for simulated image

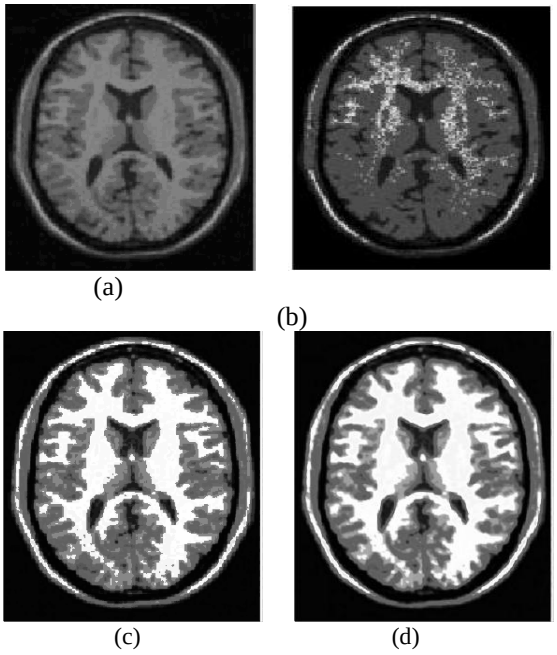

(a) (b) (c) (d)

Comparison of segmentation results on simulated T1 MRI

(a) Original image, (b) FCM, (c) BCFCM, and (d) M-

The M-FCM is more robust for noise, in above table, other columns except none can explain this point.

In addition, we segmented 32 T1 brain MR images using BCFCM and M-FCM respectively, and then we invited the experts to select better one from every image. There are twenty nine images from thirty two better images are our results of M-FCM algorithm. Although the conclusion is personality, M-FCM is better algorithm.

In studies of brain pathology, such as Multiple Sclerosis (MS), regions of interest (ROIs) that must be well defined are often examined in detail in Magnetic Resonance images (MRI). Traditionally, ROIs are outlined manually by a skilled operator using a mouse or cursor. Computer-assisted methods are used for specific applications such as extraction of MS lesions from MRI brain scans, or extraction of the cerebral ventricles in schizophrenia studies. In many cases, the computer-assisted tasks need to segment the whole brain from the head Hybrid methods that include both image-processing and prototype-based techniques are particularly effective for brain segregation. The hybrid method presented in this chapter starts with a thresholding step followed by a morphological erosion

to remove small connections between the brain and surrounding tissue.

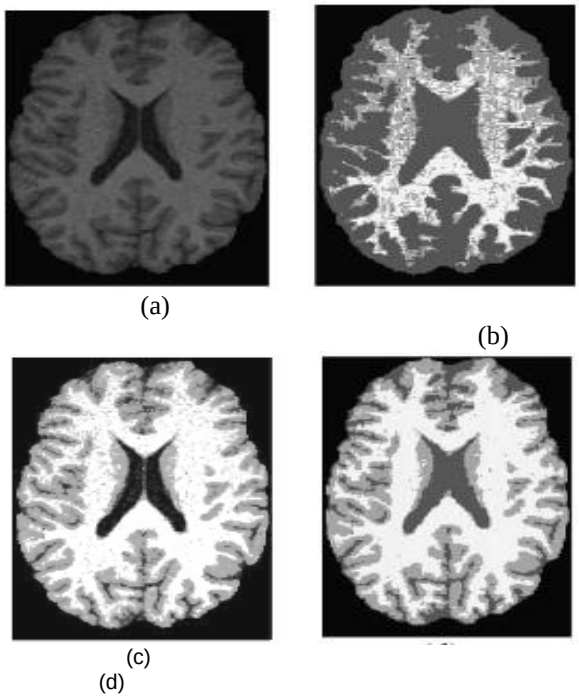

Comparison of segmentation results on real brain MRI, T1 weighted image
(a) Original image, (b) FCM, (c) BCFCM, and (d) M- FCM.

It removes eyes and other non-brain structures with a prototype-based approach followed by more image processing consisting of a morphological dilation to recover some of the eliminated tissue. A final refinement of the brain contour is achieved by an active contour algorithm . In our method, the threshold for an initial segregation is computed automatically by applying an anisotropic diffusion filter to the image and using the resulting voxel intensity histogram. The method which is based partly on 2D data and partly on 3D data operates best on routine axially-displayed multispectral dual-echo proton density (PD) and T2 (spin-spin relaxation time) sequences. This method has been successfully used to segment the brain in each slice of many head images from many different MRI scanners (all 1.5 Tesla), using several different spin-echo images with different echo times. This method also works well on axial and coronal 3D T1-weighted SPGR (Spoiled Gradient) sequences. In these images parameters have to be adjusted to ensure that the thin dark brain areas will be included and to keep the cerebellum attached to the rest of the brain which has to be separated from the back of the neck tissue and the cheeks.

4.2 Brain Segregation Method

Segregation is achieved in three stages a removal of the background using intensity histograms, generation of an initial mask that determines the intracranial boundary with a nonlinear anisotropic diffusion filter, and final segregation with an active contour prototype. The use of a visual programming environment such as WiT , makes prototype development more convenient by allowing some exploration. Preferably the T2-weighted image is used; otherwise the PD-weighted or T1-weighted image may also be used for segregation. RF in homogeneities are addressed by the smoothing obtained with the nonlinear anisotropic diffusion which also reduces the intensity of regions that do not belong to the brain. In the third stage, the relative insensitivity of the active contours to partial volume effects provides consistent edge tracking for the final segregation. This sequence of operations provides a relatively robust approach those results in good segregation even in the presence of RF in homogeneity, where simple thresholding techniques would be difficult to use.

Two types of prior knowledge are needed in the second stage, while the first and third stages do not require prior information. The first type of prior information relates to tissues other than the brain, for example the scalp and eyes. Using the anisotropic diffusion filter on T2 (or PD) images, the majority of the tissue other than the brain can be darkened, allowing a simple threshold to be used subsequently for segregation.

4.2.1 Background Removal

Considering the fact that MR scanners typically generate normally distributed white noise, the best threshold for separating background noise is determined with the technique of Bummer at all. In reconstructed MR data, background noise has a Rayleigh distribution given by:

$$p_{noise}(f) = \frac{f}{\sigma^2}\exp\left(-\frac{f^2}{2\sigma^2}\right)$$ Where f is the intensity and σ is the standard deviation of the white noise. This distribution is observed in the lower intensities of the uncorrected histogram of MR volumes as illustrated. A bimodal distribution *g(f)* is obtained if the best fit Rayleigh curve, $r(f)$, is subtracted from the volume histogram,

$$h(f) : g(f) = h(f) - r(f)$$

We can obtain a minimum error threshold, τ , by minimizing an error term, ε_r given by:

$$\varepsilon_r = \sum_{f=0}^{\tau-1} g(f) + \sum_{f=\tau}^{\times} r(f)$$

Segregation of the original image in with this automatic threshold τ produces the head mask where some misclassified pixels within the head region and speckle outside the head region are apparent. Morphological operations with a small structuring element such as a 5x5 kernel can effectively remove such noise components.

4.2.2 INITIAL BRAIN MASK

The process that generates the initial brain mask has three steps. First it smooth's the brain image using 2D nonlinear anisotropic diffusion and attenuates narrow non-brain regions. Then, it sets an automated threshold to the diffused MR volume and produces a binary mask. Third, it removes misclassified non-brain regions such as the eyes from the binary mask based on morphology and spatial information obtained from the head mask.

4.2.2.1 Nonlinear anisotropic diffusion

Nonlinear anisotropic diffusion filters introduced by Perona and Malik are tunable iterative filters that can be used to enhance MR images. Nonlinear anisotropic diffusion filters can be used also to enhance and detect object edges. The anisotropic diffusion filter is a diffusion process that facilitates intraregional smoothing and inhibits interregional smoothing:

$$\frac{\partial}{\partial t} I(\bar{x},t) = \nabla \bullet \left(c(\bar{x},t) \nabla I(\bar{x},t) \right)$$

Consider $I(\bar{x},t)$ being the MR image where $\bar{x}$ represents the image coordinates (i.e. x, y) t is the iteration step, and $c(\bar{x},t)$, Edges can be selectively smoothed or enhanced according to the diffusion function. An effective diffusion function is:

$$c(\bar{x},t) = \exp\left[-\left(\frac{\left| \nabla I(\bar{x},t) \right|}{\sqrt{2}\mathrm{K}} \right)^2 \right]$$

Where K is the diffusion or flow constant that dictates the behavior of the filter. Good choices of parameters that produce an appropriately blurred image for threshold are K = 128 with 25 iterations and a time step value of just under 0.2. Filtering can be fairly sensitive to these three parameters, however, for all the PD, T2, and T1 - weighted data sets displayed axially or corporally, the above parameter settings provide good initial brain segregation.

4.2.2.2 Automated threshold

After diffusion filtering brain voxel distribution becomes close to normal for T2-weighted and even PD images. Consequently, the threshold can be determined by fitting a Gaussian curve to the histogram of the diffused volume data. For PD and T2-weighted slices, a good threshold is set at 2 standard deviations below the mean. For T1-weighted axially-displayed images, the minimum value in the brain histogram plot is selected as the threshold. This value typically corresponds to about 0.5 standard deviations below the mean of the fitted Gaussian.

4.2.2.3 Refinement of mask

Misclassified regions, such as the eyes, that occur after automatic thresholding are removed using morphological filtering and spatial information provided by the head mask. In each region of the binary mask, first holes are filled and then binary erosion separates weakly connected regions. The width of this element is sufficient to separate the brain from the eyes in all axial slices we studied whose fields of view were between 200 and 260 mm. Two bounding boxes will be required for serially displayed images where there is no symmetry. The remaining regions are returned close to their original size with binary dilation using the same 10x10 kernel. Since thresholding eliminates the darkest pixels at the brain edge, this dilation step ensures that the mask is closer to the required edge.

4.2.3 Final Brain Mask

The final boundary between the brain and the intracranial cavity is obtained with an active contour prototype algorithm that uses the initial brain mask as its initial condition. The active contour prototype, extended from the ``Snakes" algorithm introduced by Kass et al. gradually deforms the contour of the initial brain mask to lock onto the edge of the brain. The active contour is defined as an ordered collection of n points in the image plane such that:

$$V = \{v_1, \ldots, v_n\}$$
$$v_i = (x_i, y_i), \quad i = \{1, \ldots n\}$$

An energy minimization criterion iteratively brings the points of the contour closer to the intracranial boundary. For each point, v_i, an energy matrix, $E(v_i)$, is computed:

$$E(v_i) = \alpha E_{cont}(v_i) + \beta E_{bal}(v_i) + \gamma E_{\text{int}}(v_i) + \kappa E_{grad}(v_i)$$

where $E_{cont}(v_i)$ is a ``continuity" energy function that forces the contour to take a smooth shape, $E_{bal}(v_i)$ is an adaptive ``balloon" force used to push the contour outward until a strong gradient is encountered , $E_{\text{int}}(v_i)$ is an ``intensity" energy function, computed from the PD-weighted MRI volume, that tends to move the contour towards low intensity regions, and $E_{grad}(v_i)$ is a ``gradient" energy function, computed from the diffused MRI volume, that draws the contour towards regions where the image gradient is high. Relative weights of the energy terms are provided by the scalar constants α, β, γ and κ. This procedure moves each v_i to the point of minimum energy in its neighborhood. The active contour prototype algorithm finds the intracranial boundary in all image slices using the same relative energy weightings for the combination of energy functions described above. The gradient energy term computed on the diffused volume significantly stabilizes the active contour algorithm because the gradient derivatives are small in the diffused volume data . The active contour prototype algorithm applied to the MR slice. Good results were obtained with $\alpha = 1, \beta = 2, \gamma = 1.5$, and $\kappa = 2$ on all data sets mentioned.

4.2.4 Brain Studies and Validation

PD and T2 data sets were acquired axially on a GE 1.5 Tesla MRI scanner, with repetition time TR = 2000 ms, and echo times of 35 ms and 70 ms respectively. The slice thickness was 5 mm and the pixel size was 0.781 mm^2, Each data set had 22 slices with 256 x 256 pixels per slice, and was scaled linearly from the original 12-bit data to 8-bits.

Comparable results are obtained with our algorithm on more than 30 data sets from five scanners with fields-of-view varying from 200 to 260 mm. The algorithm also works on images acquired on a GE scanner with a SPRG sequence, with TR=39 msecs and Te=8 msecs, pixel size = 1.0156 mm^2 and slice thickness = 2.5 mm. The computer processing time for each study for all the stages was less than 5 minutes on a SUN SPARC workstation – even the 120 slice 3D studies. In all cases, our algorithm detects the intracranial boundary without user interaction and without changing the parameters.

Tissue contours determined with a fully automated algorithm have to be validated with a study that compares them to contours traced manually by an expert. The similarity index described by Zijdenbos , derived from the kappa statistic can be used to compare an automated contour one drawn manually. Each binary segregation can be considered as a set A of pixels. The similarity between two segregations A_1 and A_2 is computed with a real number $S \in \{0 \cdots 1\}$ defined by

$$S = 2\frac{|A_1 \cap A_2|}{|A_1| + |A_2|}.$$

This similarity index is sensitive to both size and location since it depends on their intersection as well as the sum of their sizes. Two regions with equal size that overlap with half of their area have S=1/2 while a region that completely covers a smaller one of half its size yields S=2/3. In this manner, two regions where one fully encompasses the other are more similar than two partially overlapping regions. According to good agreement is indicated by S>0.7 but the absolute value of S may be difficult to interpret. In a validation study that we conducted, three volumes were chosen and each volume was acquired using a different PD/T2-weighted echo sequence, and a different field of view size. For each volume, some axial slices were selected, such that the entire range of the image volume from ``low'' to ``high'' slices was covered. An expert radiologist traced the brain contour manually on each slice and the manual contour was compared with the automatically drawn contour using the similarity index. Table shows the number of pixels included inside the manually drawn and automatically-calculated brain contours as well as the similarity index.

In axial slices containing the eyes, the algorithm usually included the pituitary gland and basilar artery, and sometimes the internal carotid artery, while the radiologist excluded these structures. Also, while the radiologist drew carefully around the petrous temporal bone, it was often included by the algorithm. In the high slices, manual contours were comparable to the automated ones except in the extreme case of the top slice of the 5mm thick datasets where the partial volume effect was noticeable. The sagittal sinus was usually included by the algorithm whereas it was always excluded by the radiologist.

Overall, this algorithm provided a similarity index always above 0.925, it was maximal 0.99 on middle slices, and dropped to 0.95 on the highest slices. These results compare favorably with those reported by others as the brain volumes are within 4% in most cases.

5. Result and Analysis

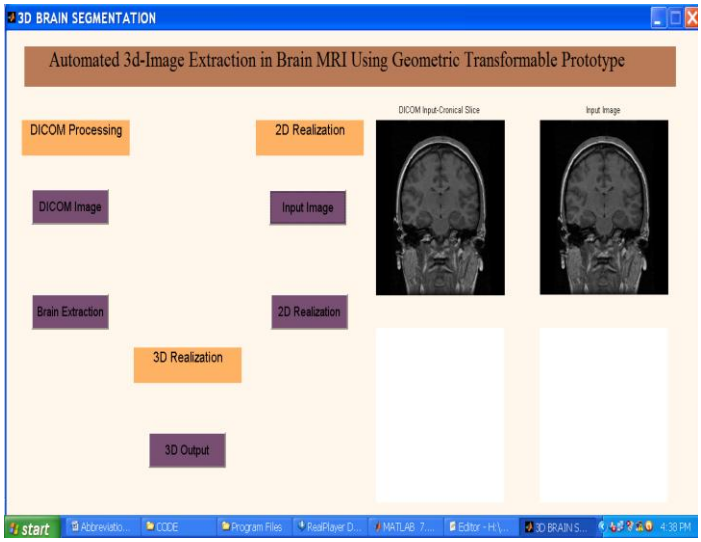

Input image

Qualitative segregation performance of two simulated T1w brain images showing the provided phantom label, raw images and the segregation results obtained by using the proposed hybrid feature. We show three slices for both the best case (0% noise, 0% in homogeneity) and worst-case (9% noise, 40%inhomogeneity) scenarios. White, light gray, and dark gray colors represent, respectively, the WM, GM, and CSF classes in the tissue and phantom labels. We note the results from the hybrid approach resemble the phantom for both the best and worst input scenarios. Segregation performance of real clinical T1w brain images (UBC MS/MRI and LONI IDA) showing the raw images and the segregation results obtained by using the proposed approach.

We show two slices each for the three-class segregation. White, light gray, and dark gray colors represent, respectively, the normal appearing WM, GM grouped with diseased WM, and CSF classes in the segregation labels. Qualitative segregation performance of a multiple simulated MR sequence(T1w, T2w, PDw) brain images showing the provided phantom label, raw images (0% noise, 0% in homogeneity), and the segregation results obtained by using the proposed approach. White, light gray and dark gray colors represent, respectively, the WM, GM, and CSF classes in the tissue and phantom labels. We show three slices for the test case and note improved segregation results on multiple MR sequence. Qualitative segregation performance of a real clinical T1w brain images (IBSR #08) showing the raw images, the expert-guided manual segregation label, and the segregation results obtained by using the traditional edge feature and the proposed hybrid approach. We show three slices for the three-class segregation case and the post processed case.

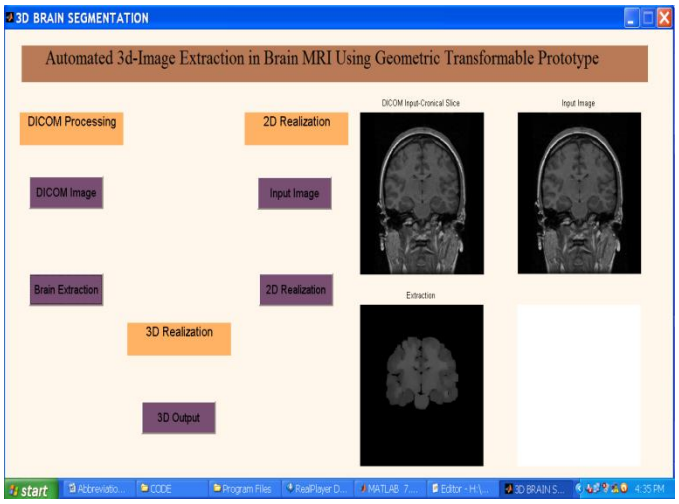

Brain Extraction

White, light gray, and dark gray colors represent, respectively, the WM, GM, and CSF classes in the segregation labels. We note the good resemblance between the segregation results and the raw image, and between the post processed results and the expert-guided manual segregation labels.

The image is converted to log-polar coordinates, its gradient is computed and the 2D segregation is recovered by finding the shortest path in the inverse of the gradient image. Fig shows the segregation in the log-polar space with highlighted contour and the corresponding contour converted to the Cartesian space image.

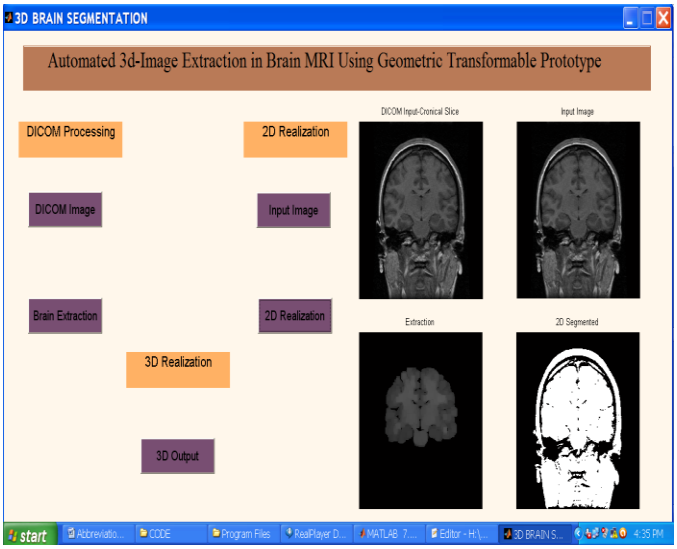

2D Realized

Once the infected area has been segmented in the interaction plane, pixels inside the lesion are used to update the lesion histogram H L and pixels within 10 pixels outside the infected area is used to generate the background histogram H B .The segmented 2D contour is recovered in the same manner on the other planes. In the case of a clicked point, the two other main MPRs (multi-planar reconstructions) are processed. In the case of a stroke, the plane that is perpendicular to the stroke plane and also contains the stroke is also processed. FIG. shows the results of the 2D segmentations 4 segmentations in image series in 4 planes for a stroke and 3 segmentations in image series in 3 planes for a click point. Since background statistics have now also been collected.

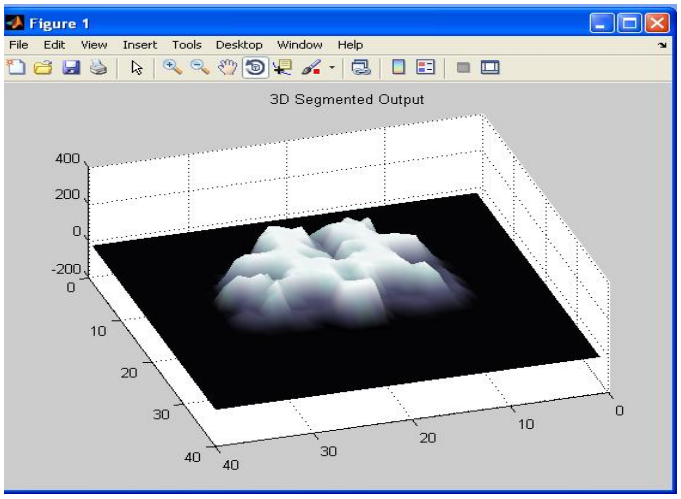

3D Segmentation

A semi-automatic 3D segmentation method for brain structures from Magnetic Resonance Imaging (MRI). There are three main contributions. First, our method combines boundary-based and region-based approaches but differs from previous hybrid methods in that we perform them in two separate phases. This allows for more efficient segregation. Second, a probability map is generated and used throughout the segregation to account for the brain structures with low-intensity contrast to the background. Third, we develop a set of tools for manual adjustment after the segregation. This is particularly important in clinical research because the reliability of the results can be ensured.

Conclusion

We validated our technique first by using both single and multiple simulated brain MRI sequence data. Improved segregation accuracy and robustness were shown in results from the proposed hybrid approach against those using individual geometric or statistical features only. Furthermore, on real clinical MRI datasets, we also demonstrated improved accuracy over a state-of-the-art approach, the region-based M3DLS. We also demonstrated consistent and robust results when segmenting MRI scans of both MS and AD patients.

MRI is the dominant neuro imaging modality for multiple sclerosis (MS). Revised diagnostic criteria formally incorporate abnormalities on MRI for diagnosis. MRI is well-suited for evaluating dynamic changes in MS patients. The suppression of new gadolinium-enhanced T1-weighted and newly active T2-weighted lesions on MRI are now standard outcome measures in clinical trials. This article reviews how conventional and advanced MRIs provide important biomarkers of MS pathology and considers the role of MRI outcomes in clinical trials and in clinical practice.

The results presented in this paper are preliminary and further clinical evaluation is required. There are also need new methods for preprocessing the original image, including de-noising and enhancing to increase the SNR. How to combine segmenting with preprocessing procedure is our work in future.

Future Work

In future we can develop a Novel Active Volume Model. Which is a natural extension of parametric transformable prototypes and it is to integrate object appearance and region information. The main contributions include: (1) a clean formulation to integrate online learning and region statistics into active contours and surfaces, which provides flexible initialization and rapid convergence, (2) the finite differences optimization framework that enables very fast gradient and appearance-statistics based model deformations, (3) the combination of multiple sources of information in a unified framework for predicting object region and boundary. Using various experiments on 3D medical images, we demonstrate that the AVM model can perform segmentation efficiently and reliably on CT and MRI images. However, due to the local smoothness of simplex-mesh, it is still hard for the model to reach details on branch structures. In the future, we plan to address this problem by re-parameterizing the model near branches since vertices. in such areas are sparser than those on the main body. We propose a principled approach for brain MRI image segmentation by fusing together adaptive atlas (generative) and informative features through a discriminative framework. This approach uses a new way of combining generative and discriminative models. It takes advantage of the generative model being explicit and the discriminative classifier having high discrimination power. We demonstrated improved and robust results over the state-of-the-art algorithms on several clinical MRI datasets. Including a more explicit shape model may further improve our system, which is left for future research.

References

[1] M. K. Beyer, C. C. Janvin, J. P. Larsen, and D. Aarsland, "An MRI study of patients with Parkinson's disease with mild cognitive impairment and dementia using voxel based morphometry," J. Neurol. Neurosurg. Psychiatry, vol. 78, no. 3, pp. 254–259, Mar. 2007.

[2] M. Grossman, C.McMillan, P.Moore, L. Ding, G. Glosser, M.Work, and J. Gee, "What's in a name: Voxel-based morphometry analysis of MRI and naming difficulty in Alzheimer's disease, frontotemporal dementia and corticobasal degeneration," Brain, vol. 127, no. 3, pp. 628–649, 2004.

[3] P. E. Grant, "StructuralMR imaging," Epilepsia, vol. 45, no. s4, pp. 4–16, 2004.

[4] J. J. Wisco, G. Kuperberg, D. Manoach, B. T. Quinn, E. Busa, B. Fischl, S. Heckers, and A. G. Sorensen, "Abnormal cortical folding patterns within Broca's area in schizophrenia: Evidence from structural MRI," Schizophrenia Res., vol. 94, no. 1–3, pp. 317–327, Aug. 2007. [5] D. W. Paty, D. Li, and G. J. Zhao,MRI in Multiple Sclerosis-Implications for Diagnosis and Treatment, 2nd ed. UBC MS/MRI Research Lab., Vancouver, BC, Canada, Rep. for Ares-Serono SA, 1999.

[6] D. H. Miller, "Biomarkers and surrogate outcomes in neurodegenerative disease: Lessons from multiple sclerosis," NeuroRx, vol. 1, pp. 284–294, 2004.

[7] A. Traboulsee, G. Zhao, and D. K. B. Li, "Neuroimaging in multiple sclerosis," Neurol. Clin., vol. 23, pp. 131–148, 2005.

[8] D. T. Chard, C. M. Griffin, G. J. M. Parker, R. Kapoor, A. J. Thompson, and D. H. Miller, "Brain atrophy in clinically early relapsing-remitting multiple sclerosis," Brain, vol. 125, no. 2, pp. 327–337, Feb. 2002.

[9] N. De Stefano, P. M. Matthews, M. Filippi, F. Agosta, M. De Luca, M. L. Bartolozzi, L. Guidi, A. Ghezzi, E. Montanari, A. Cifelli, A. Federico, and S. M. Smith, "Evidence of early cortical atrophy in MS," Neurology, vol. 60, pp. 1157–1162, 2003.

[10] J. Sastre-Garriga,G.T. Ingle, D.T. Chard, L. Ramio-Torrenta, D. H. Miller, and A. J. Thompson, "Grey and white matter atrophy in early clinical stages of primary progressive multiple sclerosis," NeuroImage, vol. 22, no. 1, pp. 353–359, May 2004.

[11] V. M. Anderson, N. C. Fox, and D. H. Miller, "Magnetic resonance imaging measures of brain atrophy in multiple sclerosis," J. Magn. Reson. Imag., vol. 23, pp. 605–618, 2006.

[12] S. K. Warfield, K. H. Zou, and W. M. Wells, "Simultaneous truth and performance level estimation (STAPLE): An algorithm for the validation of image segmentation," IEEE Trans.Med. Imag., vol. 23, no. 7, pp. 903– 921, Jul. 2004.

[13] D. L. Pham, C. Xu, and J. L. Prince, "Current methods in medical image segmentation," Annu. Rev. Biomed. Eng., vol. 2, pp. 315–337, Aug. 2000.

[14] K. M. Pohl, R. Kikinis, and W. M. Wells, "Active mean fields: Solving the mean field approximation in the level set framework," in Proc. IPMI 2007, pp. 26–37.

[15] M. Rousson, N. Paragios, and R. Deriche, "Implicit active shape models for 3D segmentation in MR imaging," in Proc. MICCAI 2004, pp. 209– 216.

[16] L. Ibanez, W. Schroeder, L. Ng, and J. Cates, The ITK Software Guide, 2nd ed. New York: Kitware, Inc., 2005.

[17] A. P. Dempster, N. M. Laird, and D. B. Rubin, "Maximum likelihood from incomplete data via the EM algorithm," J. R. Stat. Soc. Ser. B (Methodological), vol. 39, no. 1, pp. 1–38, 1977.

[18] A. Huang, R. Abugharbieh, R. Tam, and A. Traboulsee, "Automatic MRI brain tissue segmentation using a hybrid statistical and geometric model," in Proc. IEEE ISBI, 2006, pp. 394–397.

[19] R. C. Gonzales and R. E. Woods, Digital Image Processing, 2nd ed. Englewood Cliffs, NJ: Prentice-Hall, 2002, pp. 549.

[20] C.A. Cocosco et al., "BrainWeb: Online Interface to a 3D MRI Simulated Brain Database," NeuroImage, vol. 5, no. 4, part 2/4, S425, 1997 -- Proceedings of 3rd International Conference on Functional Mapping of the Human Brain, Copenhagen, May 1997.

[21] R.K.-S. Kwan et al., "MRI simulation-based evaluation of image-processing and classification methods," IEEE Transactions on Medical Imaging, vol. 18, no. 11, pp. 1085-97, November 1999.

[22] R.K.-S. Kwan, A.C. Evans, and G.B. Pike, "An Extensible MRI Simulator for Post-Processing Evaluation," Visualization in Biomedical Computing (VBC'96), Lecture Notes in computer Science, vol. 1131, pp. 135-140, Springer-Verlag, 1996.

[23]Y. Chen et al., "Using prior shapes in geometric active contours in a variational framework," International Journal of Computer Vision (IJCV), vol. 50, no. 3, pp. 315–328, 2002.

Mrs. *D Chamundeshwari,* *Assoc. Professor in Department of Electronics and Communication Engineering ,Elenki Institute of Engineering and Technology, JNTU Hyderabad, INDIA,*

E-mail: dasaris.chamu@gmail.com

Mr. *J Thirupathi*, *Assoc. Professor in Department of Computer Science and Engineering ,College of Engineering and Technology, Samara University ,Samara, ETHIOPIA,*

E-mail: thirupathij.cse@gmail.com

Mr. J Srinivas *M.Tech (Embedded Systems)II Year, RRS engineering College. JNTU Hyderabad, INDIA.*

E-mail:cnu2nice@gmail.com